Two-Parameter Kinematic Approach for Shear Strength of Deep Concrete Beams with Internal FRP Reinforcement

Boyan I. Mihaylov[1]

Abstract: Tests of deep concrete beams with internal fiber-reinforced polymer (FRP) reinforcement have shown that such members can exhibit lower shear strength than members with conventional steel reinforcement. To model this effect, the current paper proposes an approach based on a two-parameter kinematic theory (2PKT) for conventional deep beams. The 2PKT is built on a kinematic model with two degrees of freedom that describes the deformation patterns of cracked beams. Using this theory shows that large strains in FRP longitudinal reinforcement result in reduced shear resistance of the critical loading zones (CLZ) of deep beams. The original 2PKT is therefore modified by introducing a reduction factor for the shear carried by the CLZ. The extended 2PKT approach is then applied to a database of 39 tests of FRP-reinforced deep beams from the literature, resulting in an average shear strength experimental-to-predicted ratio of 1.06 and a coefficient of variation of 18.3%. The results show that the 2PKT adequately captures the effects of the stiffness of the reinforcement, section depth, concrete strength, and shear-span-to-depth ratio on the shear strength of FRP-reinforced deep beams. **DOI: 10.1061/(ASCE)CC.1943-5614.0000747.**

Author keywords: Deep beams; Fiber-reinforced polymer (FRP) reinforcement; Shear strength; Kinematic model.

Introduction

Deep reinforced concrete beams with small shear-span-to-depth ratios ($a/d \leq$ approximately 2.5) are often used to support heavy loads in bridges and other types of public infrastructure. Concerns about the durability of such structures owing to corrosion of their steel reinforcement resulted in a search for alternative solutions. One such solution, which in the last decade has been a focus of significant research activity, is the use of internal fiber-reinforced polymer (FRP) reinforcement. Compared to conventional steel reinforcement, FRP bars are not susceptible to chloride-induced corrosion and typically have higher tensile strength. At the same time, FRP reinforcement exhibits lower modulus of elasticity and brittle-elastic behavior. These properties raised questions of whether conventional methods for the design and analysis of deep beams require modifications, and whether new approaches can offer improved predictions of the shear behavior of beams with FRP reinforcement.

These issues were investigated in a number of experimental and analytical studies performed by different research groups. El-Sayed et al. (2012) used CSA-S806-11 (CSA 2011) shear provisions to predict the shear strength of eight test specimens without web reinforcement and obtained experimental-to-predicted ratios with an average of 1.33 and a coefficient of variation (COV) of 12%. The code equations became less conservative as the stiffness of the longitudinal reinforcement decreased. In a later study, Farghaly and Benmokrane (2013) applied CSA S806-12 (CSA 2012) and ACI 318-08 (ACI 2008) strut-and-tie provisions to a set of four tests. Although the CSA S806-12 (CSA 2012) provisions produced adequate results, the ACI 318-08 (ACI 2008) code was unconservative. To improve the predictions of strut-and-tie models, Nehdi et al. (2008) and Kim et al. (2014) proposed new effectiveness factors for struts in FRP-reinforced deep beams and derived the factors based on data from experimental studies involving moderate-scale test specimens (d = 150–350 mm). An extensive study on the strength modeling of deep beams with FRP reinforcement was performed by Andermatt and Lubell (2013a), who used a database of 36 moderate- and large-scale tests (d up to 889 mm) to evaluate the accuracy of five sectional models—CSA S6-06 (CSA 2006), Hoult et al. (2008), CSA S806-02 (CSA 2002), ISIS Design Manual (ISIS Canada Research Network 2007), and ACI 440.1R-06 (ACI 2006)—and three strut-and-tie models, two of which were based on CSA A23.3-04 (CSA 2004) and one on ACI 318-08 (ACI 2008). Based on the results, it was concluded that the sectional models gave poor predictions of capacity for specimens having a/d ratios smaller than 2.5. A strut-and-tie model based on the CSA A23.3-04 (CSA 2004) provisions produced most accurate strength predictions with and average experimental-to-predicted ratio of 1.20 and COV of 21%. At the same time, this model resulted in two rather unconservative predictions (experimental-to-predicted ratios $\approx$ 0.66) for specimens with high-strength concrete and $a/d \approx 2.04$. For the same two beams, the ACI 318-08 (ACI 2008) strut-and-tie provisions produced ratios as low as 0.28, and the average ratio and COV for the whole database were, respectively, 1.02 and 51%. Although all these comparisons were performed with simple strut-and-tie models applied to simply supported test specimens, caution was expressed regarding the use of strut-and-tie models for more complex members with FRP reinforcement. Because strut-and-tie models are based on the lower-bound approach of the theory of plasticity, they require that the structure possesses the ability to redistribute internal stresses and adapt to the model. In conventional deep beams, this stress redistribution is facilitated by the plastic properties of the reinforcing steel. However, because FRP reinforcement is brittle-elastic, the ability of FRP-reinforced structures to adapt to complex strut-and-tie models may be limited. Further research on this topic is recommended.

To model the brittle shear behavior of deep beams with FRP reinforcement, this paper discusses a new approach that explicitly

[1]Assistant Professor, Structural Engineering Group, Dept. of ArGEnCo, Univ. of Liege, Bât. B52, Quartier Polytech 1, Allée de la Découverte 9, 4000 Liege, Belgium. E-mail: boyan.mihaylov@ulg.ac.be

Note. This manuscript was submitted on March 30, 2016; approved on July 13, 2016; published online on August 19, 2016. Discussion period open until January 19, 2017; separate discussions must be submitted for individual papers. This paper is part of the ***Journal of Composites for Construction***, © ASCE, ISSN 1090-0268.

accounts for the deformations in the member. This approach is an extension of a two-parameter kinematic theory (2PKT) for steel-reinforced deep beams (Mihaylov et al. 2013, 2015). The 2PKT is based on a simple kinematic description of the deformations patterns of diagonally cracked members and also includes equilibrium equations and constitutive relationships for the mechanisms of shear resistance across the critical shear cracks. Because the 2PKT accounts for compatibility of deformations and the brittle behavior of the shear mechanisms, it should be possible to extend it to FRP-reinforced members without significant modifications. To identify the necessary modifications and to validate the model, results from previous experimental studies will be used.

Shear Behavior of Deep Beams with FRP Reinforcement

The shear behavior of deep beams reinforced with internal FRP bars will be discussed with the help of a test performed by Farghaly and Benmokrane (2013). The test specimen named G8N6 had an effective depth $d = 1{,}097$ mm and a shear-span-to-depth ratio $a/d = 1.14$. It was reinforced with eight No. 6 glass FRP (GFRP) bars placed on the flexural tension side of the section and had no web reinforcement. The specimen was subjected to symmetrical four-point bending up to shear failure.

The load-deflection response of specimen G8N6 is shown in Fig. 1(a) with a thin continuous line. Fig. 1(b) shows the crack diagram of the beam at shear failure. The specimen behaved linearly until the propagation of the first flexural cracks in the pure-bending region between the applied loads. Further loading caused the propagation of more flexural and flexural-shear cracks in the two symmetrical shear spans, and the stiffness of the member decreased gradually. The last cracks that developed extended from the inner edge of the supports toward the loading points along the diagonal of the shear spans (diagonal cracks). Following the propagation of these cracks, the beam was able to sustain a load increment of approximately one-third of the load that caused diagonal cracking. The diagonal cracks widened, and eventually a shear failure occurred along one of these cracks with crushing of the concrete in the vicinity of the point load. At failure, the longitudinal strains measured along the GFRP bars were almost constant from support to support as characteristic of arch action in deep beams.

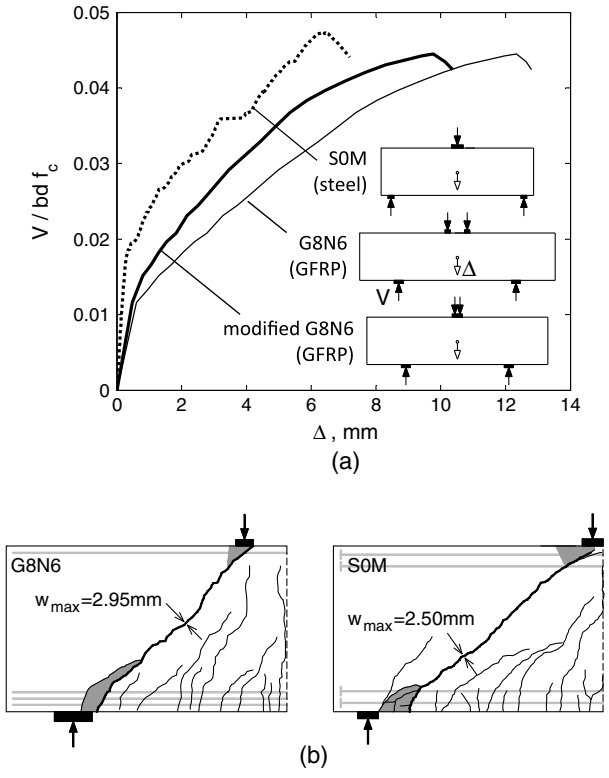

Fig. 1. Behavior of deep beams with FRP reinforcement and steel reinforcement (G8N6 data from Farghaly and Benmokrane 2013): (a) load-displacement response; (b) crack diagrams at shear failure

Qualitatively, this behavior is very similar to the behavior of steel-reinforced deep beams described in many experimental studies. It is of interest however to compare in more detail the behavior of specimen G8N6 to that of a similar deep beam with conventional steel reinforcement. Such a beam (specimen S0M) was tested at the University of Toronto under symmetrical three-point bending (Mihaylov et al. 2010). Specimen S0M had the same effective depth as G8N6 and the same reinforcement ratio $\rho_l = 0.7\%$, but was reinforced with six No. 8 steel bars instead of eight No. 6 GFRP bars. Apart from the type of reinforcement, the more significant differences between the two beams were the shear-span-to-depth ratio and the compressive strength of the concrete. Specimen G8N6 was shorter than S0M (a/d of 1.14 versus 1.55 for G8N6) and had a stronger concrete (f'_c of 49.3 MPa versus 34.2 MPa). The elastic modulus of the GFRP bars was 47.6 GPa compared to the typical value of 200 GPa for the steel reinforcement.

The load-deflection response of specimen S0M is compared to that of G8N6 in Fig. 1(a). To allow for more direct comparisons, the shear forces are normalized with respect to the effective area of the section bd and concrete strength f'_c. In addition, the deflections of specimen G8N6 are modified to take into account the different loading conditions, i.e., four-point bending for G8N6 versus three-point bending for S0M. Because specimen G8N6 had a pure bending region, the midspan deflection caused by the curvature in this region was subtracted from the total measured deflection. The curvature was evaluated based on the classical plane-sections-remain-plane approach by using the program *Response-2000* (Bentz 2000, 2009). Although the classical approach applies to slender members, it is used in this study to provide a measure of the flexural deformations between the applied loads. By comparing the thick dashed line and the thick continuous line, the two specimens are shown to exhibit different shear strengths and different deflections at peak load. Although the GFRP-reinforced specimen was significantly shorter than specimen S0M, it failed under a smaller normalized shear force and a larger midspan deflection. This result shows that the stiffness of the longitudinal reinforcement has a significant effect on the shear behavior of deep beams.

Some insight into this result can be gained from Fig. 1(b), which compares the crack diagrams of the two beams near failure. Although the two crack patterns are very similar, the GFRP-reinforced beam had a wider critical diagonal crack than the steel-reinforced member. Wider cracks result in less aggregate interlock between the crack surfaces, and therefore smaller shear capacity. The 2PKT, originally developed for members with steel reinforcement, accounts explicitly for the width of the cracks and the shear resisted by aggregate interlock, and therefore has the potential to capture the shear behavior of FRP-reinforced deep beams.

2PKT for Deep Beams and Sectional Model for Slender Beams

The two-parameter kinematic theory is built on a simple kinematic representation of the crack and deformation patterns observed in

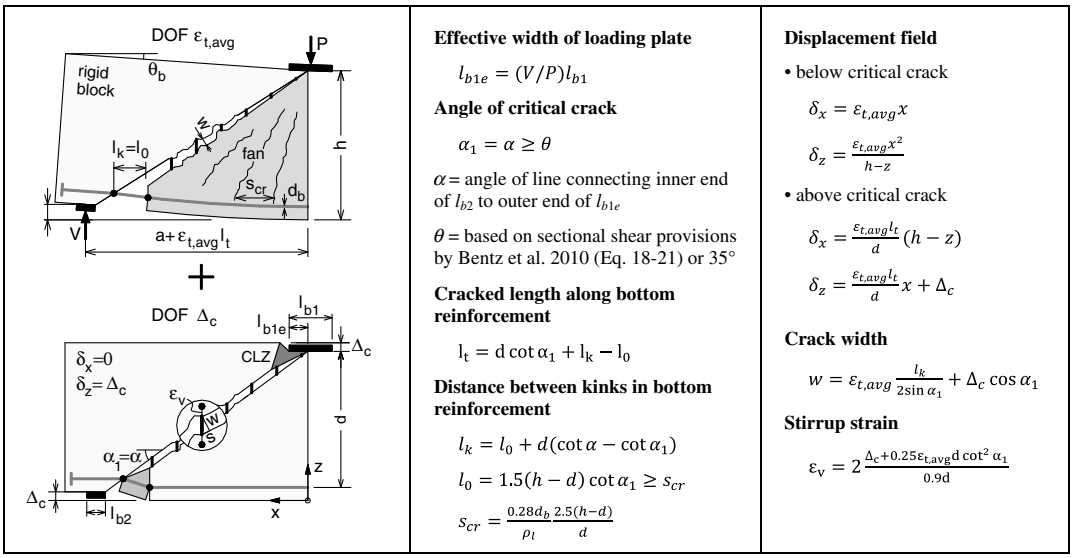

Fig. 2. Two-degree-of-freedom kinematic model for deep beams under single curvature: (a) deformation patterns and DOFs; (b) geometry; (c) deformations

deep beams (Mihaylov et al. 2011, 2013). In this approach, the critical diagonal crack is approximated with a straight line that divides the shear span in two distinct parts [Fig. 2(a)]. The concrete block above the crack is assumed rigid, whereas the concrete below the crack is marked by a series of radial flexure-shear cracks. The struts formed between these cracks are also assumed rigid, and constitute a *fan* of radial struts pinned at the loading point and connected to the bottom reinforcement. The rigid block above the critical crack rotates with respect to the vertical section at the load and translates vertically with respect to the fan. These assumptions form the basis of a kinematic model with two degrees of freedom (DOFs), which describes the entire displacement field of the critical shear span. The geometrical properties of the kinematic model are defined in Fig. 2(b), and the displacement field is given by the top four equations in Fig. 2(c) as a function of the DOFs of the model. The two DOFs are the average strain $\varepsilon_{t,\text{avg}}$ along the longitudinal reinforcement, and the vertical displacement Δ_c in the critical loading zone (CLZ), where the concrete crushes at shear failure.

Degree of freedom Δ_c is obtained based on the assumption that the CLZ is at failure under diagonal compressive stresses. Taking also into account assumptions for the geometry of the CLZ, the following expression for Δ_c has been derived:

$$\Delta_c = 0.0105 l_{b1e}\cot\alpha \tag{1}$$

where l_{b1e} = effective width of the loading plate; and α = angle of the line connecting the inner edge of the support to the outer end of l_{b1e} [Figs. 2(a and b)].

Degree of freedom $\varepsilon_{t,\text{avg}}$ can be used to express the shear force in the member based on the moment equilibrium of the shear span

$$V = E_r A_r \varepsilon_{t,\text{avg}}(0.9d)/a \tag{2}$$

where E_r = modulus of elasticity of the longitudinal reinforcement; A_r = cross-sectional area of the reinforcement; $0.9d$ = approximate lever arm of the internal forces in the section with maximum bending moment; and a = shear span. For simplicity, this equation uses the stiffness $E_r A_r$ of the bare longitudinal reinforcement and therefore neglects the tension stiffening effect of the cracked concrete around the reinforcing bars. The shear expressed with Eq. (2) can be viewed as a demand on the shear span for a given value of $\varepsilon_{t,\text{avg}}$, which at failure must equal the shear resistance along the critical diagonal crack.

In the 2PKT, the shear resistance is expressed as a sum of four components: shear carried by the critical loading zone, V_{CLZ}; aggregate interlock shear across the critical crack, V_{ci}; tension in the transverse reinforcement crossing the crack, V_s; and dowel action of the longitudinal reinforcement, V_d. It has been shown elsewhere that V_d is typically relatively small compared to the other three components (Mihaylov et al. 2013), and therefore it will be neglected in the modeling of deep beams with FRP reinforcement. This is a reasonable simplification considering also that FRP bars are significantly more flexible than steel bars. The remaining three shear strength components are expressed as follows:

$$V_{\text{CLZ}} = 1.43 k f_c'^{0.8} b l_{b1e}\sin^2\alpha \tag{3}$$

$$V_{ci} = v_{ci} b d = \frac{0.18\sqrt{f_c'}}{0.31 + \frac{24w}{a_g+16}} b d \tag{4}$$

$$V_s = E_s A_v \varepsilon_v \leq A_v f_{yv} \tag{5}$$

where k = crack shape factor given by

$$0 \leq k = 1 - 2(\cot\alpha - 2) \leq 1 \tag{6}$$

and A_v = area of the stirrups that are effective in resisting shear across the critical crack

$$A_v = \rho_v b(d\cot\alpha_1 - l_0 - 1.5 l_{b1e}) \geq 0 \tag{7}$$

Eq. (3) has been derived based on simplifying assumptions for the shape and size of the critical loading zone, as well as assumptions for the strains in the zone (Mihaylov et al. 2013). The behavior of the concrete in the CLZ has been modeled based on an appropriate stress-strain relationship for concrete under uniaxial compression (Popovics 1970). Term v_{ci} in Eq. (4) is the shear stress transferred across the critical diagonal crack by means of aggregate interlock. This stress is evaluated with an empirical expression

adopted from the modified compression field theory for elements subjected to shear (Vecchio and Collins 1986). To evaluate the shear resisted by the stirrups, an elastic perfectly plastic stress-strain relationship is used for the reinforcing steel in Eq. (5). The area of the stirrups A_v contributing to the shear resistance has been derived from the kinematic model, and accounts for the fact that the stirrups near the ends of the critical diagonal crack are not significantly strained because of the clamping effect of the support reaction and applied load. For this reason, the horizontal projection of the critical crack $d\cot\alpha_1$ used in the expression for A_v is reduced by terms l_0 near the support and $1.5l_{b1e}$ near the load [Figs. 2(a and b)].

These equations show that shear component V_{CLZ} is not a function of the DOFs of the kinematic model, whereas V_{ci} and V_s depend on Δ_c and $\varepsilon_{t,\text{avg}}$ through the width of the critical diagonal crack w and the strain in the stirrups ε_v, respectively. Deformations w and ε_v are evaluated halfway along the critical crack based on the kinematic model [see the expressions in Fig. 2(c)]. To account for strain concentration in the crack, a factor of 2 is introduced in the expression for the stirrup strain. According to Eq. (4) and the expression for w in Fig. 2(c), the larger are Δ_c and $\varepsilon_{t,\text{avg}}$, the wider is the critical diagonal crack, and the smaller is the aggregate interlock shear transferred across the crack. Regarding V_s, the larger are the two DOFs, the larger is the strain in the stirrups, and the larger is the shear resisted by the stirrups if they remain elastic. Because the steel reinforcement is assumed to have an elastic perfectly plastic behavior, shear component V_s cannot exceed the yield strength of the stirrups $A_v f_{yv}$.

To demonstrate how Eqs. (1)–(7) are solved together with the equations in Fig. 2, the 2PKT approach will be applied without modifications to a deep beam with GFRP reinforcement (specimen A1/50) (Latosh 2014). The beam was subjected to symmetrical three-point bending similarly to specimen S0M. The effective depth of the beam was 621 mm, and the a/d ratio was 1.0. The ratio of longitudinal reinforcement was 1.19%, whereas the stirrups ratio was 0.061%. The solution of the equations of the 2PKT approach for this beam is demonstrated graphically in Fig. 3. On the horizontal axis of the plot is DOF $\varepsilon_{t,\text{avg}}$, and on the vertical axis are the shear forces. DOF Δ_c is calculated in advance from Eq. (1) and equals 0.74 mm. The thick dashed line in the plot shows the shear force derived from the moment equilibrium of the shear span [Eq. (2)], which increases linearly because of the linear behavior of the longitudinal reinforcement. The thick continuous line on the other hand represents the shear capacity along the critical diagonal crack. This capacity equals the sum of shear components V_{CLZ}, V_{ci}, and V_s [Eqs. (3)–(5)], which are also plotted in Fig. 3. As the shear forces must be in equilibrium, the solution of the 2PKT equations lies at the intersection of the two thick lines. This intersection can be found by using the bisection method or by a trial-and-error procedure. For specimen A1/50 the intersection is at $\varepsilon_{t,\text{avg}}$ of 8.42×10^{-3}, which is approximately four times larger than the yield strain of typical reinforcing steel. The GFRP bars however remained elastic under this strain because they had an ultimate strain of approximately 14×10^{-3}. The shear corresponding to $\varepsilon_{t,\text{avg}}$ of 8.42×10^{-3} equals 615 kN, and represents the 2PKT prediction for the shear strength of the beam.

To ensure that this is the final prediction, it is also necessary to calculate the shear strength based on a sectional model for slender beams. Sectional models are aimed at capturing the breakdown of beam action, which in deep beams is followed by the development of a stronger load-bearing mechanism, arch action. Therefore, the final shear strength prediction will be the maximum of the predictions of the sectional model and the 2PKT approach. The sectional model adopted in this study was proposed by Bentz et al. (2010)

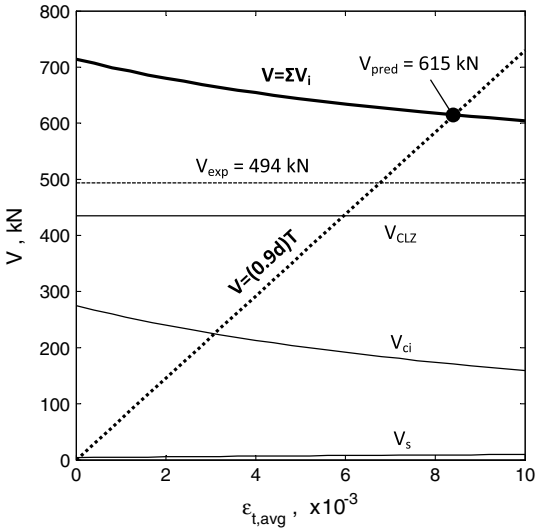

Fig. 3. 2PKT approach applied to GFRP-reinforced specimen A1/50 (data from Latosh 2014)

based on the simplified modified compression field theory (Bentz et al. 2006). Other suitable models based on the same theory have been implemented in the Canadian highway bridge design code (CSA 2006) and in the Canadian code for design and construction of building structures with fiber-reinforced polymers (CSA 2012; Razaqpur and Spadea 2015). Similarly to the 2PKT, these approaches account explicitly for the effect of the strains in the longitudinal reinforcement on the shear strength. The equations of the model by Bentz et al. (2006) for beams with less than minimum shear reinforcement are summarized as follows for convenience:

$$V=\frac{0.3}{0.5+(500\varepsilon_t+0.15)^{0.7}}\frac{1{,}300}{1{,}000+s_{xe}}\sqrt{f_c'}b(0.9d) \quad (8)$$

$$\varepsilon_t=V\frac{\max[M/(V0.9d),1]+1}{E_rA_r} \quad (9)$$

$$s_{xe}=\frac{31.5d}{16+a_g}\geq 0.77d \quad (10)$$

$$\theta=(29^\circ+3{,}500\varepsilon_t)(0.88+s_{xe}/2{,}500)\leq 75^\circ \quad (11)$$

where V = shear strength; ε_t = strain in the longitudinal reinforcement in the critical section; s_{xe} = effective crack spacing; M = bending moment in the critical section; and θ = angle of the critical shear crack with respect to the longitudinal axis of the beam. The critical section is located at a distance of $0.9d$ from the edge of the loading element, but not farther than one-half of the clear shear span. The minimum shear reinforcement ratio in slender beams can be calculated from the CSA S806-12 (CSA 2012) code as $0.07\sqrt{f_c'}/(0.4f_{Fu})$, where f_{Fu} is the ultimate tensile strength of the stirrups. Strength f_{Fu} is calculated at the bends of the stirrups and depends on the radius of the bent: the smaller is the radius, the weaker is the FRP stirrup. If the shear reinforcement ratio is smaller than the minimum ratio, the contribution of the stirrups to the shear resistance is neglected as evident from Eq. (8).

Similarly to the 2PKT, Eqs. (8)–(11) require an iterative solution procedure based on varying strain ε_t. The solution of the sectional model for specimen A1/50 is demonstrated graphically in Fig. 4. The shear demand on the critical section is expressed from Eq. (9),

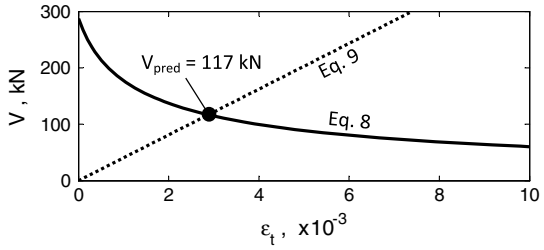

Fig. 4. Sectional model by Bentz et al. (2010) applied to GFRP-reinforced specimen A1/50 (data from Latosh 2014)

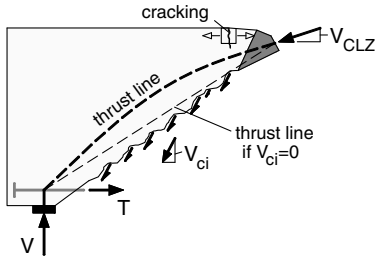

Fig. 5. Effect of position of thrust line in deep beams

whereas the shear capacity is calculated from Eq. (8). The intersection of the demand and capacity curves gives a shear strength prediction of 117 kN. This value is significantly smaller than the 2PKT prediction of 615 kN, and therefore the final prediction is $V_{\text{pred}} = 615$ kN. Although this is not a surprising result for a deep beam such as A1/50 ($a/d = 1.0$), the sectional prediction can govern for members in the transition zone from deep to slender beams ($a/d = 2 - 3$). Therefore, the sectional model adopted in this study is necessary for defining the limit of applicability of the proposed kinematic approach for deep beams. The final prediction of 615 kN exceeds the measured shear strength of specimen A1/50 $V_{\text{exp}} = 494$ kN (see thin dashed line in Fig. 3). The shear strength experimental-to-predicted ratio $V_{\text{exp}}/V_{\text{pred}}$ is $494/615 = 0.80$.

To understand the reasons for this unconservative prediction, it is necessary to analyze the three components of shear resistance plotted in Fig. 3. It can be seen that component V_s increases linearly with $\varepsilon_{t,\text{avg}}$, indicating that the stress in the stirrups do not exceed the ultimate stress of the GFRP bars. This component has a negligible contribution to the shear strength of specimen A1/50, and therefore can be disregarded as a source of the error. Component V_{ci} decreases with increasing strains in the longitudinal reinforcement as a result of the widening of the critical diagonal crack. Because this component accounts explicitly for the effect of large strains in GFRP-reinforcement, it can also be disregarded as a primary source of the unconservative prediction. Therefore, it can be concluded that the shear carried in the critical loading zone is overestimated by the original 2PKT approach. Although the 2PKT assumes that V_{CLZ} is not affected by the flexural strains, the results in Fig. 3 indicate that this component must decrease as $\varepsilon_{t,\text{avg}}$ increases.

Modifications to the Original 2PKT Approach

The reduction in shear capacity of the critical loading zones with increasing flexural strains can be devoted to two phenomena. The first phenomenon has to do with the rotation of the rigid block above the critical diagonal crack [see angle θ_b in Fig. 2(a)]. This rotation is derived from the kinematic model and equals $\varepsilon_{t,\text{avg}} \cot \alpha$. Because θ_b is proportional to the average strain in the longitudinal reinforcement, deep beams with FRP bars will typically exhibit larger rotations than steel-reinforced beams. It is likely that large rotations cause additional damage in the critical loading zones, and therefore reduce their capacity to carry shear. The second phenomenon has to do with the position of the thrust line in the rigid block (Fig. 5). The thrust line represents the flow of compressive stresses from the load to the support. Large rotations of the rigid block will result in wider diagonal cracks, and therefore less aggregate interlock shear V_{ci}. If V_{ci} is negligible, the thrust line will be nearly aligned with the bottom face of the CLZ, and this can cause cracking along the top face. Premature failures of the CLZ resulting from such cracking have been observed in tests of FRP-reinforced deep beams without shear reinforcement (Andermatt and Lubell 2013b). If however the diagonal cracks are narrow and the aggregate interlock is significant as in steel-reinforced deep beams, the thrust line will be curved upward and the tension in the top of the CLZ will diminish. In such cases the CLZ will develop its full capacity governed by concrete crushing.

The full crushing capacity of the CLZ can also develop in FRP-reinforced members with large amounts of transverse reinforcement. The transverse reinforcement (stirrups) will reduce the rotations of the rigid block, and therefore will reduce the damage in the CLZ associated with rotations. More importantly, the tension force in the stirrups will shift the thrust line in the rigid block closer to its top edge, and in this way will reduce the likelihood of premature failure of the CLZ. As it will be shown subsequently however, tests of deep beams with large amounts of FRP web reinforcement are very limited, and therefore these assumptions need to be verified in future experimental studies.

Because the explicit modeling of the described phenomena can significantly complicate the 2PKT, it is suggested to adopt a semi-empirical approach to modify shear contribution V_{CLZ}. For this purpose, a database of 39 tests of deep beams with FRP reinforcement was collected from five experimental studies (Andermatt and Lubell 2013b; El-Sayed et al. 2012; Farghaly and Benmokrane 2013; Latosh 2014; Mohamed et al. 2014). Only test series that contained at least several relatively large beams, i.e., $d > 300$ mm, were selected to avoid the inherent scatter in smaller members. All available test series featured specimens with rectangular cross sections. The properties of the tests are summarized in Table 1, which also lists the observed failure modes and measured shear resistances V_{exp}. The a/d ratio of the beams varies from 0.92 to 2.07, the effective depth d from 257 to 1,111 mm, the ratio of longitudinal reinforcement ρ_l from 0.26 to 2.13%, the ratio of transverse reinforcement (stirrups) ρ_v from 0 to 0.42%, and the concrete compressive strength f'_c from 37.0 to 68.5 MPa.

To evaluate shear component V_{CLZ} with the help of the database, it is first necessary to obtain DOF $\varepsilon_{t,\text{avg}}$ by using Eq. (2), which is solved for $\varepsilon_{t,\text{avg}}$ by substituting the shear force V with the measured shear resistance V_{exp}. Because DOF Δ_c is not directly measured in tests and is not expressed with the shear force, it is calculated from Eq. (1). With these values of the DOFs of the kinematic model, shear components V_{ci} and V_s are calculated from Eqs. (4) and (5). The shear carried by the CLZ is then calculated by subtracting V_{ci} and V_s from the measured shear strengths V_{exp}. Finally, Eq. (3) for V_{CLZ} is used to calculate the value of factor k for each of the tests in the database. This procedure ensures that if the 2PKT approach is used with the obtained k factors, it will produce shear strengths equal to those measured in the tests.

The obtained k factors are plotted in Fig. 6 as a function of the rotation of the rigid block $\theta_b = \varepsilon_{t,\text{avg}} \cot \alpha$. The plot also shows results for steel-reinforced deep beams from earlier studies (Mihaylov et al. 2013). Most of the steel-reinforced specimens had rotations less than 0.005 rad, whereas most FRP-reinforced specimens had

Table 1. Database of Deep Beam Tests with Internal FRP Reinforcement

Numbers	References	Beam name	a/d	b (mm)	d (mm)	h (mm)	a (mm)	l_{b1} (mm)	l_{b2} (mm)	V/P	E_r (GPa)	ρ_l (%)	Number of bars	f_u (MPa)	a_g (mm)	f'_c (MPa)	ρ_v (%)	d_{bv} (mm)	f_{uv} (MPa)	E_s (GPa)	ρ_h (%)	Reported mode	V_{exp} (kN)	V_{pred} (kN)	Experimental/ predicted
1	Andermatt	A1N	1.07	310	257	306	276	100	100	1	41.1	1.49	3	709	14	40.2	0	—	—	—	0	F	407.0	305.8	—
2	and Lubell	A2N	1.44	310	261	310	376	100	100	1	41.1	1.47	3	709	14	45.4	0	—	—	—	0	S	235.5	205.7	1.14
3	(2013b)	A3N	2.02	310	261	310	527	100	100	1	41.1	1.47	3	709	14	41.3	0	—	—	—	0	S	121.5	116.1	1.05
4		A4H	2.02	310	261	310	527	100	100	1	41.1	1.47	3	709	14	64.6	0	—	—	—	0	S	96.0	130.0	0.74
5		B1N	1.08	300	503	608	545	200	200	1	37.9	1.70	8	765	14	40.5	0	—	—	—	0	F	636.5	592.1	—
6		B2N	1.48	300	501	606	743	200	200	1	37.9	1.71	8	765	14	39.9	0	—	—	—	0	S	399.5	363.8	1.10
7		B3N	2.07	300	502	607	1,040	200	200	1	37.9	1.71	8	765	14	41.2	0	—	—	—	0	S	215.5	209.7	1.03
8		B4N	1.48	300	496	606	736	200	200	1	41.1	2.13	8	709	14	40.7	0	—	—	—	0	S	415.0	431.6	0.96
9		B5H	1.48	300	497	607	736	200	200	1	41.1	2.12	8	709	14	66.4	0	—	—	—	0	S	531.0	501.9	1.06
10		B6H	2.06	300	505	610	1,040	200	200	1	37.9	1.70	8	765	14	68.5	0	—	—	—	0	S	188.0	240.6	0.78
11		C1N	1.10	301	889	1,003	974	330	330	1	42.3	1.58	8	938	14	51.6	0	—	—	—	0	S	1,134.5	1,026.7	1.10
12		C2N	1.49	304	891	1,005	1,329	330	330	1	42.3	1.56	8	938	14	50.7	0	—	—	—	0	S	662.0	625.0	1.06
13	El-Sayed	C-0.7/1.6	1.69	250	326	400	550	100	100	1	134.0	0.78	5	986	20	39.4	0	—	—	—	0	S	179.5	197.6	0.91
14	et al. (2012)	G-0.7/1.6	1.69	250	326	400	550	100	100	1	42.0	0.78	5	749	20	40.5	0	—	—	—	0	S	164.5	108.6	1.51
15		C-1.2/1.6	1.69	250	326	400	550	100	100	1	134.0	1.25	8	986	20	39.4	0	—	—	—	0	S	195.0	250.3	0.78
16		G-1.2/1.6	1.69	250	326	400	550	100	100	1	42.0	1.25	8	749	20	40.5	0	—	—	—	0	S	175.0	144.5	1.21
17		C-1.7/1.6	1.69	250	326	400	550	100	100	1	134.0	1.71	11	986	20	39.4	0	—	—	—	0	S	233.5	285.6	0.82
18		G-1.7/1.6	1.69	250	326	400	550	100	100	1	42.0	1.71	11	749	20	40.5	0	—	—	—	0	S	196.0	170.4	1.15
19		C-1.2/1.3	1.30	250	326	400	425	100	100	1	134.0	1.25	8	986	20	39.4	0	—	—	—	0	S	372.0	363.7	1.02
20		G-1.2/1.3	1.30	250	326	400	425	100	100	1	42.0	1.25	8	749	20	40.5	0	—	—	—	0	S	269.0	211.9	1.27
21		C-1.2/0.9	0.92	250	326	400	300	100	100	1	134.0	1.25	8	986	20	40.0	0	—	—	—	0	F		541.0	—
22		G-1.2/0.9	0.92	250	326	400	300	100	100	1	42.0	1.25	8	749	20	40.0	0	—	—	—	0	F	450.5	341.2	—
23	Farghaly and	G8N6	1.14	300	1,097	1,200	1,250	130	228	1	47.6	0.69	8	790	20	49.3	0	—	—	—	0	S	723.5	593.5	1.22
24	Benmokrane	G8N8	1.15	300	1,088	1,200	1,250	130	228	1	51.9	1.24	8	750	20	49.3	0	—	—	—	0	S	953.0	796.5	1.20
25	(2013)	C12N3	1.13	300	1,111	1,200	1,250	130	228	1	120.0	0.26	12	1,596	20	38.7	0	—	—	—	0	S	595.5	528.6	1.13
26		C12N4	1.13	300	1,106	1,200	1,250	130	228	1	144.0	0.46	12	1,899	20	38.7	0	—	—	—	0	S	800.5	741.2	1.08
27	Latosh	A1/100	1.00	230	621	675	621	180	180	0.5	47.6	1.19	6	656	14	49.8	0.141	6.4	874	46.1	0.073	S	560.3	492.8	1.14
28	(2014)	A1/75	1.00	230	621	675	621	180	180	0.5	47.6	1.19	6	656	14	52.2	0.095	6.4	874	46.1	0.045	S	552.4	498.1	1.11
29		A1/50	1.00	230	621	675	621	180	180	0.5	47.6	1.19	6	656	14	52.5	0.061	6.4	874	46.1	0.045	S	493.7	496.5	0.99
30		A1/00	1.00	230	621	675	621	180	180	0.5	47.6	1.19	6	656	14	52.7	0	—	—	—	0	S	416.9	492.6	0.85
31		B1.5/100	1.50	230	447	500	671	180	180	0.5	47.2	1.21	6	692	14	51.8	0.141	6.4	874	46.1	0.069	S	322.4	252.4	1.28
32		C2/100	2.00	230	328	375	656	180	180	0.5	46.3	1.03	6	708	14	50.8	0.158	6.4	874	46.1	0.102	S	125.9	146.8	0.86
33		C2/75	2.00	230	328	375	656	180	180	0.5	46.3	1.03	6	708	14	51.0	0.095	6.4	874	46.1	0.102	S	98.7	130.9	0.75
34		C2/50	2.00	230	328	375	656	180	180	0.5	46.3	1.03	6	708	14	51.3	0.061	6.4	874	46.1	0	S	102.7	122.7	0.84
35		C2/00	2.00	230	328	375	656	180	180	0.5	46.3	1.03	6	708	14	51.3	0	—	—	—	0	S	93.5	109.9	0.85
36	Mohamed	G8-8	1.13	300	1,106	1,200	1,250	203	233	1	66.4	1.22	8	1,000	20	37.0	0	—	—	—	0	S	1,344	883.8	1.52
37	et al. (2014)	G8-8H	1.13	300	1,106	1,200	1,250	203	233	1	66.4	1.22	8	1,000	20	44.6	0	—	—	—	0.677	S	1,266	957.0	1.32
38		G8-8V	1.13	300	1,106	1,200	1,250	203	233	1	66.4	1.22	8	1,000	20	44.6	0.422	12.7	941	53.6	0	S	1,618	1,497.6	1.08
39		G8-8VH	1.13	300	1,106	1,200	1,250	203	233	1	66.4	1.22	8	1,000	20	37.0	0.422	12.7	941	53.6	0.677	S	1,452	1,341.3	1.08
																								Average all	= 1.06
																								COV all	= 18.3%
																								Average $d > 350$ mm	= 1.10
																								COV $d > 350$ mm	= 14.2%

Note: F = flexure; S = shear.

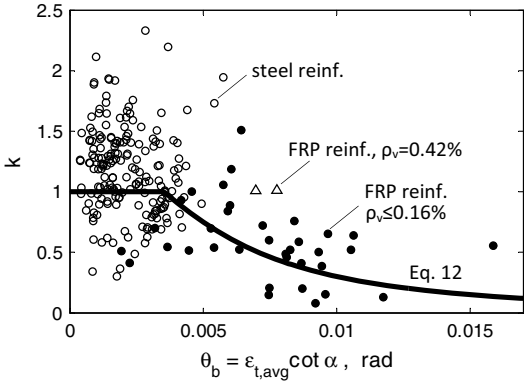

Fig. 6. Reduction factor for shear component V_{CLZ}

θ_b in excess of 0.005 rad. Despite the significant scatter in the results, it is evident that the two sets of data follow a continuous trend: k decreases with increasing θ_b, particularly when the rotation exceeds 0.005 rad. This continuous trend demonstrates that the original 2PKT for steel-reinforced deep beams can be extended to members with FRP reinforcement. The scatter of the results in Fig. 6 is devoted in part to the approximate nature of the equations of the 2PKT, and in part to natural variations in material and geometrical properties. As shown elsewhere (Mihaylov et al. 2010; Mihaylov 2015), random variations in the path of the critical diagonal crack in the vicinity of the load can cause significant scatter in the shear behavior of the critical loading zones, i.e., variations in shear strength of up to 60%. Furthermore, the CLZ can be affected by the way the load is applied on the beam (columns, steel plates, or other), by the presence of top longitudinal reinforcement, and by other factors.

In the original 2PKT approach, factor k is expressed with $\cot\alpha \approx a/d$ and accounts for the shape of the critical cracks [Eq. (6)]. It equals 1.0 for deep beams with $\cot\alpha \le 2.0$ and decreases linearly to zero as $\cot\alpha$ increases from 2.0 to 2.5. This relationship reflects the fact that in slender beams with $a/d >$ 2.5–3.0, the critical crack is not straight, but has an s-shape. Because of this shape, the crack approaches the load at a flat angle, resulting in a slender CLZ with a negligible shear resistance. Based on the results presented in Fig. 6, it is suggested to modify factor k to account not only for the crack shape, but also for the strains in the longitudinal reinforcement by using $\theta_b = \varepsilon_{t,\text{avg}} \cot\alpha$ as a governing parameter. The following expression is proposed to approximate the trend indicated by the data points:

$$k = \frac{1.5}{1 + (200\varepsilon_{t,\text{avg}} \cot\alpha)^2} \le 1.0 \tag{12}$$

where the upper limit of 1.0 allows the extended 2PKT approach to transition to the original approach when the rotations of the rigid block are relatively small. This expression is shown with a continuous line in Fig. 6.

Eq. (12) was derived mostly from beams without shear reinforcement or with very small amount of reinforcement. Of the 39 specimens in Table 1, 30 had no stirrups and seven had $0.06\% \le \rho_v \le 0.16\%$. These ratios are significantly smaller than the minimum ratios of 0.3 and 0.4% recommended in the CSA S806-12 (CSA 2012) code for GFRP- and CFRP-reinforced deep beams, respectively. However, as mentioned previously regarding Fig. 5, if the amount of stirrups exceeds a certain minimum amount, the degradation of the CLZ with increasing block rotations is expected to greatly diminish. To account for this effect in a simple manner, it is suggested that the k factor for beams with $\rho_v > 0.30\%$ is calculated from Eq. (6) of the original 2PKT approach. The limit ratio of 0.30% is proposed as a preliminary value until more experimental data becomes available. The database in Table 1 contains only two specimens with $\rho_v > 0.30\%$: G8-8V and G8-8VH with $\rho_v = 0.42\%$. As evident from the two triangular markers in Fig. 6, the ideal value of the k factor for these two beams is close to 1. The same value is obtained from Eq. (6) of the original 2PKT.

Apart from factor k, a second necessary modification of the original 2PKT approach concerns shear component V_s in members with FRP stirrups. According to Eq. (5) for the shear carried by transverse reinforcement, the stress in the reinforcement remains constant after the steel yields. However, because FRP reinforcement behaves linearly up until it breaks, such an elastic-plastic model is not appropriate. Furthermore, as mentioned previously, the breaking stress of FRP stirrups is not constant along their length, but is lower at the bends of the stirrups. To capture the brittle behavior of FRP stirrups, it is suggested to use a linear stress-strain relationship with a sudden drop to zero stress at strain f_{uv}/E_s

$$V_s = E_s A_v \varepsilon_v \quad \text{if } \varepsilon_v \le f_{uv}/E_s \tag{13}$$

$$V_s = 0 \quad \text{if } \varepsilon_v > f_{uv}/E_s$$

where E_s = modulus of elasticity of the FRP stirrups; A_v = area of effective stirrups [Eq. (7)]; ε_v = strain in the stirrups halfway along the critical crack [Fig. 2(c)]; and f_{uv} = breaking stress. Based on the displacement field equations of the kinematic model [Fig. 2(c)], the strains in the stirrups are shown to vary parabolically along the critical crack. At the ends of the crack, the strains are almost zero, whereas the maximum strain develops halfway along the crack. As mentioned previously regarding stirrup area A_v, this uneven strain distribution is accounted for by neglecting the stirrups in the vicinity of the support and loading points. It therefore follows from Eq. (13) that V_s is estimated as the product of the maximum stirrup stress and a reduced stirrup area. This is a conservative formulation, because V_s is predicted to drop to zero when the most stressed stirrup reaches its breaking stress. Because this occurs in the middle of the critical diagonal crack away from the bends of the stirrups, it is suggested to use the breaking stress f_{uv} of the straight portions of the stirrups. This suggestion can also be partially justified with the stress concentration factor of 2 used in the expression for strain ε_v [Fig. 2(c)]. However, until further experimental research is performed on deep beams with FRP stirrups, these recommendations should be considered as tentative.

With the two proposed modifications, the 2PKT approach is applied again to specimen A1/50 for which the original 2PKT produced a $V_{\text{exp}}/V_{\text{pred}}$ ratio of 0.80. This is illustrated in Fig. 7, which has the same axes as Fig. 3. The thick continuous line in the plot shows that now the shear resistance decreases more rapidly with increasing strains in the flexural reinforcement owing to the modified k factor. As a result, the intersection of the shear resistance and shear demand lines is very close to the horizontal dashed line representing the measured shear strength of specimen A1/50 ($V_{\text{exp}}/V_{\text{pred}} = 0.99$).

The extended 2PKT approach and the sectional model by Bentz et al. (2010) were also applied to the entire database of 39 FRP-reinforced deep beams. The results are summarized in Fig. 8, where on the horizontal axis are the measured shear strengths, and on the vertical axis are the corresponding 2PKT predictions. In all cases the 2PKT produced larger shear strengths than the sectional model, and therefore the kinematic approach governed the final predictions. In addition, in all cases of beams with transverse reinforcement the stress in the stirrups was predicted to remain below the breaking stress f_{uv}, and thus shear component V_s was not zero.

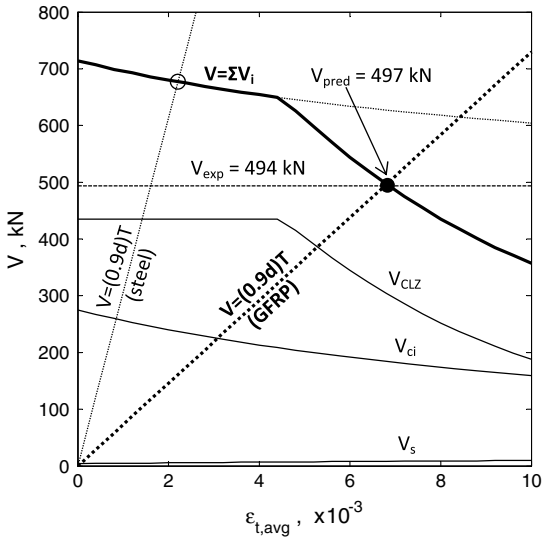

Fig. 7. Extended 2PKT approach applied to GFRP-reinforced specimen A1/50 (data from Latosh 2014)

Fig. 8 shows that the data points are well grouped along the diagonal of the plot, particularly in the range of larger shear forces corresponding to larger test specimens. The predicted shear strengths are listed in Table 1 together with the corresponding $V_{\text{exp}}/V_{\text{pred}}$ ratios. The average value of these ratios is 1.06 and the COV is 18.3%. If only specimens with effective depths larger than 350 mm are considered (20 beams), the average ratio and COV become 1.10 and 14.2%. These latter results are consistent with those obtained with the 2PKT for steel-reinforced deep beams: an average of 1.10 and a COV of 13.7% for a database of 434 tests (Mihaylov et al. 2013). It is therefore recommended to limit the applicability of the extended 2PKT approach to members with $d > 350$ mm, which are more representative of real structural members.

Because the 2PKT approach provides estimates of crack widths at failure, it is also of interest to compare these widths to test measurements. Twenty tests from the database involved the measuring of the width of the critical diagonal cracks halfway along the cracks (Andermatt and Lubell 2013b; Farghaly and Benmokrane 2013; Mohamed et al. 2014). For these tests, the model produced crack width experimental-to-predicted ratios with an average of 1.23 and a COV of 39.6%. Although the scatter in the ratios is significant as typical of crack widths, the 2PKT provides reasonable crack-width estimates necessary for evaluating the shear resisted by aggregate interlock.

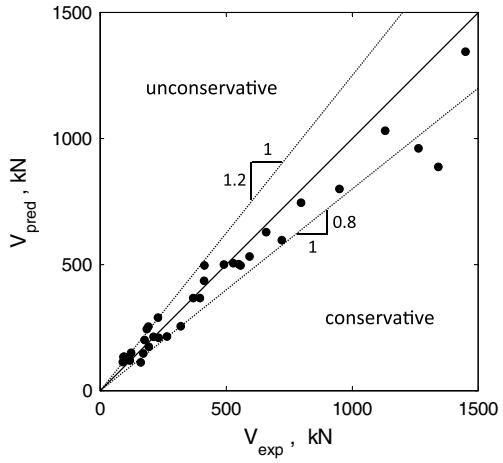

Fig. 8. Results from extended 2PKT approach for the shear strength deep beams with FRP reinforcement

Effect of Test Variables on the Shear Strength of FRP-Reinforced Deep Beams

Although the earlier comparisons showed the overall statistical behavior of the extended 2PKT, it is also of interest to evaluate the effectiveness of this approach in capturing the effect of different variables on the shear strength of FRP-reinforced deep beams. The subsequent sections are therefore focused on more detailed comparisons with individual test series from the database in Table 1.

Effect of Reinforcement Stiffness

As discussed previously, FRP reinforcement is characterized by significantly lower stiffness than conventional steel reinforcement (see E_r in Table 1). It is therefore of interest to study how the stiffness of the longitudinal reinforcement alone influences the shear strength of deep beams. An appropriate set of tests for this purpose are beams G8N6, G8N8, C12N3, and C12N4 tested by Farghaly and Benmocrane (2013). The former two beams had glass FRP bottom reinforcement with a modulus of elasticity of approximately 50 GPa, whereas the latter had carbon FRP bars with E_r of approximately 132 GPa. In addition to the type of longitudinal reinforcement, the authors also varied its ratio ρ_l from 0.26 to 1.24%. Fig. 9 shows the relationship between the shear strength of the specimens and the stiffness of the longitudinal reinforcement expressed with the product of E_r and ρ_l. The experimental points show that pairs of specimens with very similar stiffness parameters $E_r\rho_l$, but different types of FRP bars, had almost identical shear strengths. Also, the measured shear strengths increased by approximately 25% as $E_r\rho_l$ was doubled from approximately 320 to 640 MPa. For comparison, a typical steel-reinforced deep beam can have a stiffness parameter of the order of 1,400–1,800 MPa. The thick continuous line in the plot shows that the 2PKT approach captures well the trend indicated by the experimental points, although it slightly underestimates the shear capacity of the specimens. It is predicted that the increase of shear strength is a result of the increase of shear components V_{CLZ} and V_{ci}, and V_s is zero because the beams had no web reinforcement. Larger reinforcement stiffness is predicted to result in smaller rotations of the rigid block and narrower critical

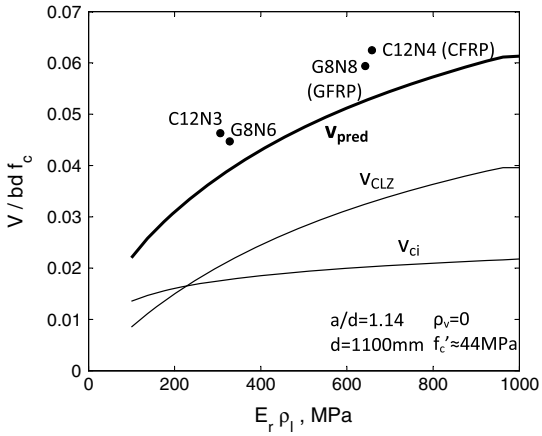

Fig. 9. Effect of reinforcement stiffness (data and 2PKT predictions from Farghaly and Benmokrane 2013)

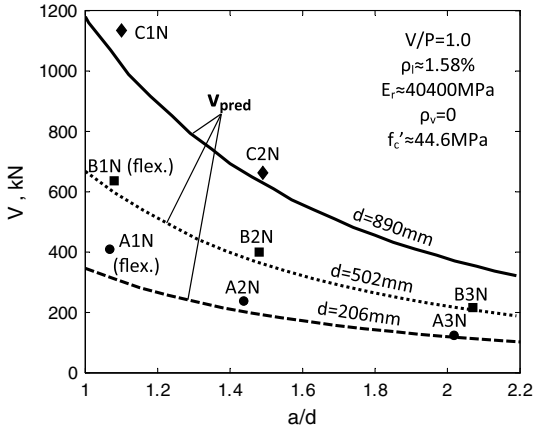

Fig. 10. Effect of section depth and shear-span-to-depth ratio (data and 2PKT predictions from Andermatt and Lubell 2013a)

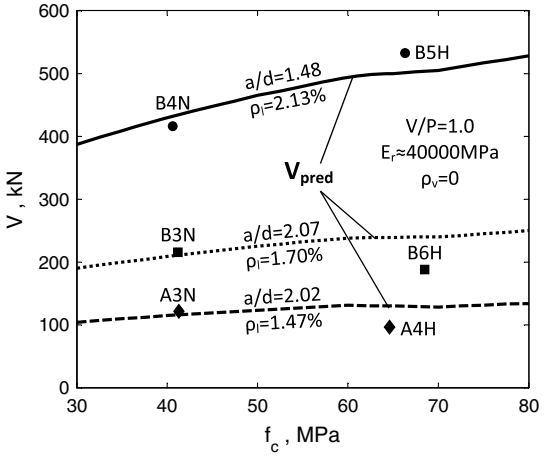

Fig. 11. Effect of concrete compressive strength (data and 2PKT predictions from Andermatt and Lubell 2013a)

cracks, which in turn results in stronger CLZ and aggregate interlock mechanisms.

The way the 2PKT approach accounts for the stiffness of the longitudinal reinforcement is demonstrated graphically in Fig. 7. The shear capacity curve in the plot will remain unchanged for beams with different stiffness parameter $E_r\rho_l$ because shear components V_{CLZ}, V_{ci}, and V_s do not depend on the longitudinal reinforcement. On the other hand, the thick dashed line—which shows the shear expressed from the tension force in the bottom reinforcement—becomes steeper [Eq. (2)]. Therefore as $E_r\rho_l$ increases, the intersection of the shear capacity and shear demand curves will occur at smaller strains and higher shear forces.

Effect Shear-Span-To-Depth Ratio and Section Depth

The shear-span-to-depth ratio a/d is a primary parameter affecting the shear strength of deep beams. This can be demonstrated very clearly with the test series performed by Andermatt and Lubell (2013b), who tested beams without shear reinforcement subjected to symmetrical four-point bending. Fig. 10 shows the shear strength of the test specimens plotted as a function of the a/d ratio. Three sets of beams with different effective depths were tested (d of 206, 502, and 890 mm), and the a/d ratio for each set was varied by changing the span of the beam. The experimental points for beams with $d = 502$ mm show that the shear strength decreased approximately three times as a/d was increased from 1.07 to approximately 2.07. This trend is also adequately captured by the 2PKT approach. As can be expected, specimens with a deeper section had larger shear strengths. If the shear strengths are plotted in terms of average shear stress at failure $v = V/bd$, the three sets of experimental points and prediction lines become almost overlapping. This result can be interpreted as evidence that deep beams do not exhibit size effect in shear. However, because not all beam dimensions were scaled equally, these test results do not allow for a strong conclusion in this regard.

Effect of Concrete Compressive Strength

The test series by Andermatt and Lubell (2013b) allow the effect of the concrete compressive strength on the shear capacity of FRP-reinforced deep beams to be studied. Three pairs of tests were performed in which the primary difference between the pairs was the a/d ratio ($a/d = 1.48$, 1.70, and 2.07) (Fig. 11). The compressive strength of the concrete in each pair of tests was varied from approximately 41 to 66 MPa. The plot shows that the increase of compressive strength resulted in an increased shear strength of the beams with a/d of 1.48, whereas for the more slender beams, this trend was slightly reversed. Therefore, for beams with a/d of 2.02 and 2.07, the increase of concrete compressive strength resulted in a slight decrease in shear capacity. This observation is somewhat counterintuitive because, in principle, higher compressive strength should result in higher shear strengths. The experimental results however seem slightly less surprising when viewed together with the 2PKT predictions. The model captures well the increase of shear strength in the beams with a/d of 1.48 and predicts an almost flat trend for the more slender beams. It is therefore expected that natural scatter in the experiments can offer a partial explanation of the decreasing trend. More importantly however, the authors of the tests observed that the critical cracks in specimens A4H and B6H had an s-shape, and the beams failed with cracking at the top of the critical loading zone as illustrated in Fig. 5. The proposed modified factor k for the CLZ is aimed at capturing these effects in an approximate manner.

Summary and Conclusions

This paper presented a kinematics-based approach for evaluating the shear strength of deep beams with internal FRP reinforcement. This approach is an extension of a 2PKT for the shear behavior of deep beams with steel reinforcement (Mihaylov et al. 2013). The 2PKT is based on a simple description of the deformation patterns in deep beams, and accounts for four mechanisms of shear resistance: shear carried in the CLZ, aggregate interlock, shear resisted by stirrups, and dowel action of the longitudinal reinforcement. The dowel action was neglected in the modeling of FRP-reinforced beams, whereas the original expressions for the shear carried by the CLZ and stirrups were modified to account for the low stiffness and brittle behavior of FRP reinforcement.

The low stiffness of FRP reinforcement results in large flexural strains, which cause damage in the critical loading zone of the beam through complex mechanisms. Because the explicit modeling of these mechanisms can significantly complicate the 2PKT approach, a simple expression was proposed for reducing the shear capacity of the CLZ with increasing strains in the longitudinal reinforcement.

The brittle behavior of FRP bars can have an unfavorable effect on the shear carried by stirrups. The most strained stirrups can rupture suddenly and cause a zipper-type failure along the diagonal crack. Considering the lack of sufficient experimental data on deep

beams with FRP web reinforcement, it was suggested to neglect the contribution of the stirrups if the maximum strain in them is predicted to exceed the ultimate strain of the material.

With the aforementioned modifications, the 2PKT approach was applied to the specimens from the database resulting in an average shear strength experimental-to-predicted ratio of 1.06 and a COV of 18.3%. When only specimens with effective depths larger than 350 mm were considered, the average ratio became 1.10 and the COV improved to 14.2%. The extended 2PKT was shown to adequately capture the effects of the stiffness of the longitudinal reinforcement, section depth, shear-span-to-depth ratio, and concrete strength on the shear strength of large deep beams. Further research is however needed for a more explicit modeling of the complex phenomena related to the low stiffness and brittle behavior of FRP reinforcement in deep beams.

Notation

The following symbols are used in this paper:

A_r = area of longitudinal bars on the flexural tension side;
A_v = area of stirrups resisting shear;
a = shear span from center of load to center of support;
a_g = maximum size of coarse aggregate;
b = width of cross section;
d = effective depth of section;
d_b = diameter of bottom longitudinal bars;
d_{bv} = stirrup diameter;
E_r = modulus of elasticity of longitudinal reinforcement;
E_s = modulus of elasticity of stirrups;
f'_c = concrete cylinder strength;
f_{Fu} = ultimate strength of FRP stirrups according to CSA S806-12;
f_u = ultimate strength of FRP longitudinal reinforcement;
f_{uv} = ultimate strength of FRP stirrups;
f_{yv} = yield strength of steel stirrups;
h = total depth of section;
k = crack shape factor;
l_0 = length of heavily cracked zone at the bottom of the critical diagonal crack;
l_{b1} = width of loading plate parallel to longitudinal axis of member;
l_{b1e} = effective width of loading plate parallel to longitudinal axis of member;
l_{b2} = width of support plate parallel to longitudinal axis of member;
l_k = length of dowels provided by bottom longitudinal reinforcement;
l_t = cracked length along bottom reinforcement;
M = bending moment at critical section;
P = applied point load;
s = crack slip;
s_{cr} = distance between radial cracks along bottom longitudinal reinforcement;
s_{xe} = effective crack spacing;
T = tensile force in bottom reinforcement;
V = shear force;
V_{CLZ} = shear resisted by the CLZ;
V_{ci} = shear resisted by aggregate interlock;
V_d = shear resisted by dowel action;
V_{exp} = measured shear strength;
V_{pred} = predicted shear strength;
V_s = shear resisted by stirrups;
w = width of critical crack;
α = angle of line extending from the inner edge of support plate to the far edge of the tributary area of the loading plate responsible for the shear force V;
α_1 = angle of critical diagonal crack;
Δ = midspan deflection of beam;
Δ_c = shear distortion of critical loading zone;
δ_x = displacement along x-axis;
δ_z = displacement along z-axis;
ε_t = strain in bottom longitudinal reinforcement in the critical section;
$\varepsilon_{t,avg}$ = average strain along bottom longitudinal reinforcement;
ε_v = transverse web strain;
θ = angle of diagonal cracks in uniform stress field;
θ_b = rotation of rigid block;
ρ_l = ratio of bottom longitudinal reinforcement;
ρ_h = ratio of horizontal web reinforcement; and
ρ_v = ratio of transverse reinforcement.

References

ACI (American Concrete Institute). (2006). "Guide for the design and construction of concrete reinforced with FRP bars." *ACI 440.1R-06*, Farmington Hills, MI.

ACI (American Concrete Institute). (2008). "Building code requirements for structural concrete and commentary." *ACI 318-08*, Farmington Hills, MI.

Andermatt, M. F., and Lubell, A. S. (2013a). "Behavior of concrete deep beams reinforced with internal fiber-reinforced polymer—Experimental study." *ACI Struct. J.*, 110(4), 585–594.

Andermatt, M. F., and Lubell, A. S. (2013b). "Strength modeling of concrete deep beams reinforced with internal fiber-reinforced polymer." *ACI Struct. J.*, 110(4), 595–606.

Bentz, E. C. (2000). "Sectional analysis of reinforced concrete members." Ph.D. thesis, Dept. of Civil Engineering, Univ. of Toronto, ON, Canada.

Bentz, E. C. (2009). "Response-2000 sectional analysis program." ⟨http://www.ecf.utoronto.ca/~bentz/r2k.htm⟩ (Mar. 17, 2015).

Bentz, E. C., Massam, L., and Collins, M. P. (2010). "Shear strength of large concrete members with FRP reinforcement." *J. Compos. Constr.*, 10.1061/(ASCE)CC.1943-5614.0000108, 637–646.

Bentz, E. C., Vecchio, F. J., and Collins, M. P. (2006). "Simplified modified compression field theory for calculating shear strength of reinforced concrete members." *ACI Struct. J.*, 103(4), 614–624.

CSA (Canadian Standards Association). (2002). "Design and construction of building components with fibre-reinforced polymers." *CAN/CSA S806-02*, Mississauga, ON, Canada.

CSA (Canadian Standards Association). (2004). "Design of concrete structures standard." *CAN/CSA A23.3-04*, Mississauga, ON, Canada.

CSA (Canadian Standards Association). (2006). "Canadian highway bridge design code." *CAN/CSA S6-06*, Mississauga, ON, Canada.

CSA (Canadian Standards Association). (2011). "Design and construction of building components with fibre reinforced polymers." *CAN/CSA S806-11*, Mississauga, ON, Canada.

CSA (Canadian Standards Association). (2012). "Design and construction of building components with fiber-reinforced polymers." *CAN/CSA S806-12*, Mississauga, ON, Canada.

El-Sayed, A., El-Salakawy, E. F., and Benmokrane, B. (2012). "Shear strength of FRP-reinforced concrete deep beams without web reinforcement." *Can. J. Civ. Eng.*, 39(5), 546–555.

Farghaly, A., and Benmokrane, B. (2013). "Shear behavior of FRP-reinforced concrete deep beams without web reinforcement." *J. Compos. Constr.*, 10.1061/(ASCE)CC.1943-5614.0000385, 04013015.

Hoult, N. A., Sherwood, E. G., Bentz, E. C., and Collins, M. P. (2008). "Does the use of FRP reinforcement change the one-way shear behavior of reinforced concrete slabs?" *J. Compos. Constr.*, 10.1061/(ASCE)1090-0268(2008)12:2(125), 125–133.

ISIS Canada Research Network. (2007). "Reinforcing concrete structures with fibre reinforced polymers—Design manual 3, version 2." Winnipeg, MB, Canada.

Kim, D., Lee, J., and Lee, Y. (2014). "Effectiveness factor of strut-and-tie model for concrete deep beams reinforced with FRP rebars." *Composites Part B*, 56, 117–125.

Latosh, F. A. (2014). "Structural behaviour of conventional and FRP-reinforced concrete deep beams." Ph.D. thesis, Dept. of Building, Civil, and Environmental Engineering, Concordia Univ., Montreal, QC, Canada.

Mihaylov, B. I. (2015). "Five-spring model for complete shear behaviour of deep beams." *FIB Struct. Concr.*, 16(1), 71–83.

Mihaylov, B. I., Bentz, E. C., and Collins, M. P. (2010). "Behavior of large deep beams subjected to monotonic and reversed cyclic shear." *ACI Struct. J.*, 107(6), 726–734.

Mihaylov, B. I., Bentz, E. C., and Collins, M. P. (2011). "A two degree of freedom kinematic model for predicting the deformations of deep beams." *Annual Conf. of the Canadian Society for Civil Engineering*, Vol. 2, Curran Associates, Red Hook, NY, 1040–1049.

Mihaylov, B. I., Bentz, E. C., and Collins, M. P. (2013). "Two-parameter kinematic theory for shear behavior of deep beams." *ACI Struct. J.*, 110(3), 447–456.

Mihaylov, B. I., Hunt, B., Bentz, E. C., and Collins, M. P. (2015). "Three-parameter kinematic theory for shear behavior of continuous deep beams." *ACI Struct. J.*, 112(1), 47–57.

Mohamed, K., Farghaly, A. S., and Benmokrane, B. (2014). "Effect of web reinforcement in FRP-reinforced deep beams." *7th Int. Conf. on FRP Composites in Civil Engineering*, International Institute for FRP in Construction, Vancouver, Canada.

Nehdi, M., Omeman, Z., and EI-Chabib, H. (2008). "Optimal efficiency factor in strut-and-tie model for FRP-reinforced concrete short beams with $(1.5 < a/d < 2.5)$." *Mater. Struct.*, 41(10), 1713–1727.

Popovics, S. (1970). "A review of stress-strain relationships for concrete." *ACI J. Proc.*, 67(3), 243–248.

Razaqpur, A. G., and Spadea, S. (2015). "Shear strength of FRP reinforced concrete members with stirrups." *J. Compos. Constr.*, 10.1061/(ASCE)CC.1943-5614.0000483, 04014025.

Vecchio, F. J., and Collins, M. P. (1986). "The modified compression field theory for reinforced concrete elements subjected to shear." *ACI Struct. J.*, 83(2), 219–231.